46th AIAA Aerospace Sciences Meeting and Exhibit
Jan 7 – 10, 2008, Reno, Nevada
AIAA-2008-0315

An Experimental Investigation on Aerodynamic Hysteresis of a Low-Reynolds Number Airfoil

Zifeng Yang[1], Hirofumi Igarashi[2], Mathew Martin[3] and Hui Hu[4](✉)

Iowa State University, Ames, Iowa, 50011

An experimental study was conducted to investigate the aerodynamic characteristics of a NASA low speed GA(W)-1 airfoil at the chord Reynolds number of Re_C=160,000. Aerodynamic hysteresis was observed for the angles of attack close to the static stall angle of the airfoil. In addition to mapping surface pressure distribution around the airfoil, a high-resolution PIV system was used to make detailed flow field measurements to quantify the occurrence and behavior of laminar boundary layer separation and transition on the airfoil when aerodynamic hysteresis occurs. The flow field measurements were correlated with the airfoil surface pressure measurements to elucidate underlying fundamental physics. For the same angle of attack in hysteresis loop, the flow obtained along the increasing angle branch was found to result in an almost attached flow with small unsteadiness, higher lift and lower drag, whereas the one with decreasing angle of attack branch was associated with large unsteadiness, lower lift, and higher drag. The hysteresis was found to be closely related to the behavior of the laminar boundary layer separation and transition on the airfoil. The ability of the flow to remember its past history is believed to be responsible for the hysteretic behavior.

I. Introduction

LOW-REYNOLDS-NUMBER airfoil aerodynamics is important for both military and civilian applications. The applications include propellers, sailplanes, ultralight man-carrying/man-powered aircraft, high-altitude vehicles, wind turbines, unmanned aerial vehicles (UAVs), and micro air vehicles (MAVs). For the applications listed, the combination of small length scale and low flight velocities results in airfoils operating at low chord Reynolds numbers of Re_C < 500,000.

It is well known that many significant aerodynamic problems occur for low-Reynolds number airfoils with their chord Reynolds numbers less than 500,000 [1]. Hysteresis phenomena have been found to be relatively common for round nosed airfoils at low Reynolds numbers. Aerodynamic hysteresis of an airfoil refers to airfoil aerodynamic characteristics as it becomes history dependent, i.e., dependent on the sense of change of the angle of attack, near the airfoil stall angle. The coefficients of lift, drag, and moment of the airfoil are found to be multiple-valued rather than single-valued functions of the angle of attack in hysteresis loop. Aerodynamic hysteresis is of practical importance because it produces widely different values of lift coefficient and lift-to-drag ratio for a given airfoil at a given angle of attack. It could also affect the recovery from stall and/or spin flight conditions. Whereas aerodynamic hysteresis associated with the pitching motion of airfoils (also known as dynamic stall) has been investigated extensively as summarized in the review article of McCorskey [2], hysteresis phenomena observed for static stall of an airfoil have received much less attention.

Pohlen and Mueller [3] and Mueller [4] investigated the aerodynamic characteristics of Miley M06-13-128 and Lissaman 7769 airfoils at low Reynolds numbers, and found both airfoils produced aerodynamic hysteresis loops in the profiles of measured lift and drag forces when they operated below chord Reynolds numbers of 300,000. Based on qualitative flow visualization with smoke, Mueller [4] suggested that airfoil hysteresis is closely related to

[1] Graduate Student, Department of Aerospace Engineering.
[2] Graduate Student, Department of Aerospace Engineering.
[3] Undergraduate Student, Department of Aerospace Engineering.
[4] Assistant Professor, Department of Aerospace Engineering, and AIAA Senior Member, email: huhui@iastate.edu.

laminar boundary layer transition and separation on the airfoils. Hoffmann [5] studied the aerodynamic characteristics of a NACA 0015 airfoil at a chord Reynolds number of 250,000, and hysteresis loop was observed in the measured coefficients of drag and lift. He also found that hysteresis could be observed for low free stream turbulence cases (up to ~ 2% turbulence intensity) but disappeared for high free stream turbulence cases. Biber and Zumwalt [6] reported that aerodynamic hysteresis phenomena occur for not only single-element airfoils but also multi-element airfoil configurations. More recently, Mittal and Saxena [7] conducted a numerical study to predict the aerodynamic hysteresis near the static stall angle of a NACA 0012 airfoil in comparison with the experimental data of Thibert et al. [8].

Although it has been suggested that aerodynamic hysteresis is closely related to the laminar boundary layer separation and transition on low-Reynolds-number airfoils, detailed flow field measurements have never been carried out to confirm the conjectures. Very little can be found in literature to elucidate the relation between the aerodynamic hysteresis phenomena observed in the measured aerodynamic (lift, drag and moment) coefficients with the flow pattern and the behavior of vortex and turbulent flow structures around the airfoils. In the present study, we report the measurement results of a detailed experimental study to investigate aerodynamic hysteresis near the static stall angle of a low-Reynolds-number airfoil. In addition to mapping surface pressure distribution around the airfoil with pressure sensors, a high-resolution particle image velocimetry (PIV) system was used to make detailed flow field measurements to quantify the occurrence and behavior of laminar boundary layer separation and transition on the airfoil when aerodynamic hysteresis occurs. The detailed flow field measurements were correlated with the airfoil surface pressure measurements to elucidate underlying fundamental physics associated with the aerodynamic hysteresis observed in the measured aerodynamic (lift and drag) coefficient profiles. To the best knowledge of the authors, this is the first effort of its nature. The primary objective of the present study is to gain further insight into fundamental physics of aerodynamic hysteresis of low-Reynolds-number airfoils. In addition, the quantitative measurements will be used as the database for the validation of computational fluid dynamics (CFD) simulations of such complicated flow phenomena for the optimum design of low-Reynolds-number airfoils.

II. Studied Airfoils and Experimental Setup

The experiments were performed in a closed-circuit low-speed wind tunnel located in the Aerospace Engineering Department of Iowa State University. The tunnel has a test section with a 1.0 ft × 1.0 ft (30 cm × 30 cm) cross section and optically transparent walls. The tunnel has a contraction section upstream of the test section with honeycomb, screen structures, and cooling system installed ahead of the contraction section to provide uniform low turbulent incoming flow to enter the test section.

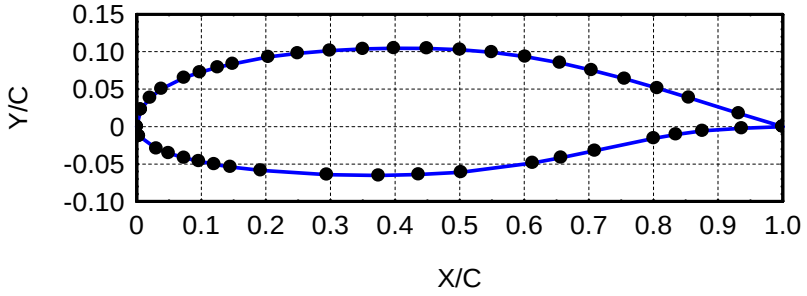

Fig 1. GA(W)-1 airfoil geometry and pressure tap locations

Figure 1 shows the schematic of the airfoil used in the present study: a GA (W)-1 airfoil (also labeled as NASA LS(1)-0417). The GA (W)-1 has a maximum thickness of 17% of the chord length. Compared with standard NACA airfoils, the GA (W)-1 airfoil was specially designed for low-speed general aviation applications with a large leading-edge radius in order to flatten the peak in pressure coefficient near the airfoil nose to discourage flow separation [20]. The chord length of the airfoil model is 101mm, i. e., C = 101mm, for the present study. The flow velocity at the inlet of the test section was set as U_∞ = 24 m/s, which corresponds to a chord Reynolds number of Re_C = 160,000. The turbulence intensity of the incoming stream was found to be within 1.0%, measured by using a hot-wire anemometer.

The airfoil model was equipped with 43 pressure taps at its median span with the spanwise length of the airfoil being 1.0 ft. The locations of the pressure taps are indicated in Fig. 1. The 43 pressure taps were connected by plastic tubing to 43 channels of a pressure acquisition system (model DSA3217, Scanivalve Corp). The DSA3217 digital sensor arrays incorporate temperature compensated piezo-resistive pressure sensors with a pneumatic calibration valve, RAM, 16 bit A/D converter, and a microprocessor in a compact self-contained module. The precision of the pressure acquisition system is ± 0.2% of the full scale (± 10 inch H_2O). During the experiment, each pressure transducer input was scanned at 400 Hz for 20 seconds. The pressure coefficient distributions, C_P , around the airfoil at various angles of attack were measured by using the pressure acquisition system. The lift and drag coefficients, C_l and C_d, of the 2-D airfoil were determined by numerically integrating the pressure distribution around the airfoil. It should be noted that the drag coefficient of an airfoil is composed of two parts, the pressure drag component (which comes from the fore and aft unbalance in the pressure distribution around the airfoil) and the skin friction component (which comes from the viscous surface stresses around the airfoil). At low angles of attack skin friction dominates the total drag while the pressure drag component is minor. At high angles of attack the reverse occurs. Since skin friction drag component was ignored in the present study, as a result, the drag coefficient of the airfoil was underestimated. The underestimation of the aerodynamic drag could be significant for the cases at low angles of attack. However, since aerodynamic hysteresis of an airfoil is usually found to occur at high angles of attack (near airfoil stall angle), pressure drag component is significant and skin friction drag is negligible when aerodynamic hysteresis occurs. In the present study, all the coefficient data were corrected for wind tunnel blockages [9].

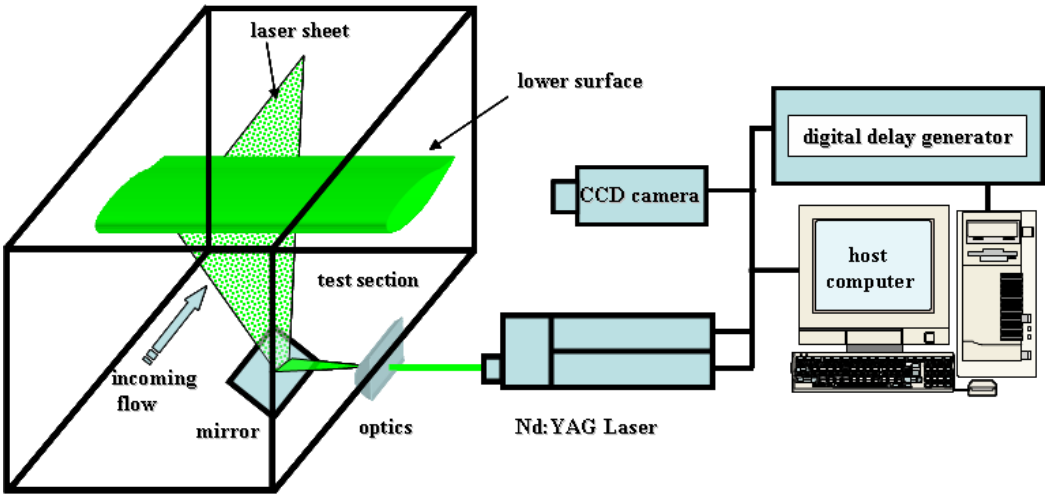

Fig. 2. Schematic of the experimental setup for the PIV measurements

Figure 2 shows the schematic of the experimental setup used for the PIV measurements. The test airfoil was installed in the middle of the test section. A PIV system was used to make flow velocity field measurements along the chord at the middle span of the airfoil. The flow was seeded with ~ 1 μm oil droplets. Illumination was provided by a double-pulsed Nd:YAG laser (NewWave Gemini 200) adjusted on the second harmonic and emitting two laser pulses of 200 mJ at a wavelength of 532 nm with a repetition rate of 10 Hz. The laser beam was shaped to a laser sheet (thickness ~1 mm) by using a set of mirrors, spherical and cylindrical lenses. A high resolution 12-bit (1376×1040 pixels, SensiCam, Cooke Corp.) charge-coupled device (CCD) camera was used for PIV image acquisition with its axis perpendicular to the laser sheet. The CCD camera and the double-pulsed Nd:YAG lasers were connected to a workstation via a digital delay generator, which controlled the timing of the laser illumination and the image acquisition.

Instantaneous PIV velocity vectors were obtained by using a frame-to-frame cross correlation technique with interrogation windows of 32 ×32 pixels. An effective overlap of 50% of the interrogation windows was employed for the PIV image processing. After the instantaneous velocity vectors (u_i, v_i) were determined, the spanwise

vorticity (ϖ_z) could be derived. The time-averaged quantities such as mean velocity (U,V), turbulent velocity fluctuations ($\overline{u'}$, $\overline{v'}$), and normalized turbulent kinetic energy ($T.K.E. = (\overline{u'^2} + \overline{v'^2})/U_\infty^2$) were obtained from a cinema sequence of 400 frames of instantaneous velocity fields. The measurement uncertainty level for the velocity vectors is estimated to be within 2.0%, and that of TKE is about 5.0%.

III. Experimental Results and Discussions

A. Aerodynamic force measurement results

Figure 3 shows the profiles of the measured lift and drag coefficients versus angle of attack (AOA). Hysteresis in the aerodynamic coefficients can be observed clearly for the angles of attack lying between 13.0 and 16.0 degrees. With the increasing angle of attack, airfoil stall was found to occur at AOA =15.0 deg, while for the decreasing angle it occurs at AOA = 13.0 deg. The hysteresis loop was found to be clockwise in the lift coefficient profiles, and counter-clockwise in the drag coefficient profiles. The aerodynamic hysteresis resulted in significant variations of lift coefficient, C_l, and lift-to-drag ratio, l/d, for the airfoil at a given angle of attack. For example, the lift coefficient and lift-to-drag ratio at AOA = 14.0 degrees were found to be C_l = 1.33 and l/d = 23.5 when the angle is at the increasing angle branch of the hysteresis loop. The values were found to become C_l = 0.8 and l/d = 3.66 for the same 14.0 degrees angle of attack when it is at the deceasing angle branch of the hysteresis loop.

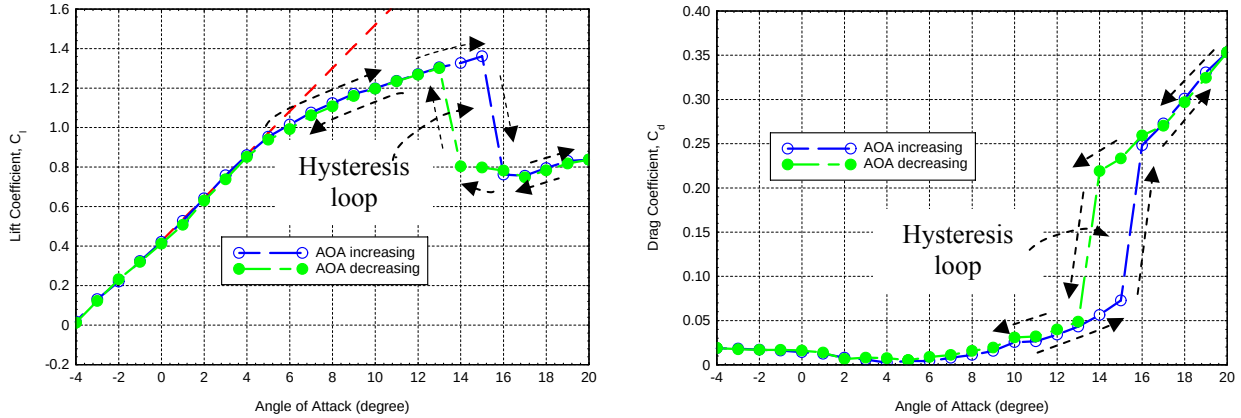

a. lift coefficient b. drag coefficient

Fig. 3. Measured lift and drag coefficients versus the angle of attack.

Figure 4 shows the measured surface pressure coefficient distributions around the airfoil as the angle of attack of the airfoil changing from 12.0 to 17.0 degrees along both the increasing and decreasing branches of the hysteresis loop. It can be seen clearly that, while the surface pressure distributions on the airfoil lower surface do not change very much, the surface pressure distributions on the airfoil upper surface were found to vary significantly for the same angles of attack (AOA= 14.0 and 15.0 degrees) in the hysteresis loop with the angles being reached along the increasing angle branch of the hysteresis loop compared with those along decreasing angle branch of the hysteresis loop. When the AOA=14.0 and 15.0 degrees are at the increasing angle branch of the hysteresis loop, the surface pressure coefficient profiles along the airfoil upper surface was found to reach its negative peak rapidly at a location near to the airfoil leading edge, then, the surface pressure recovers over the airfoil upper surface, which are very similar as those cases with AOA =12.0 and 13.0 degrees. A region of nearly constant pressure (i.e., "plateau" region) was found at the locations of $X/C \approx 0.05$ with a sudden increase in surface pressure following the "plateau" region. Further downstream of $X/C > 0.15$, surface pressure was found to recover gradually and smoothly. Such a feature of the surface pressure coefficient profiles is actually closely related to laminar boundary layer separation and transition, and formation of laminar separation bubbles on low-Reynolds-number airfoils.

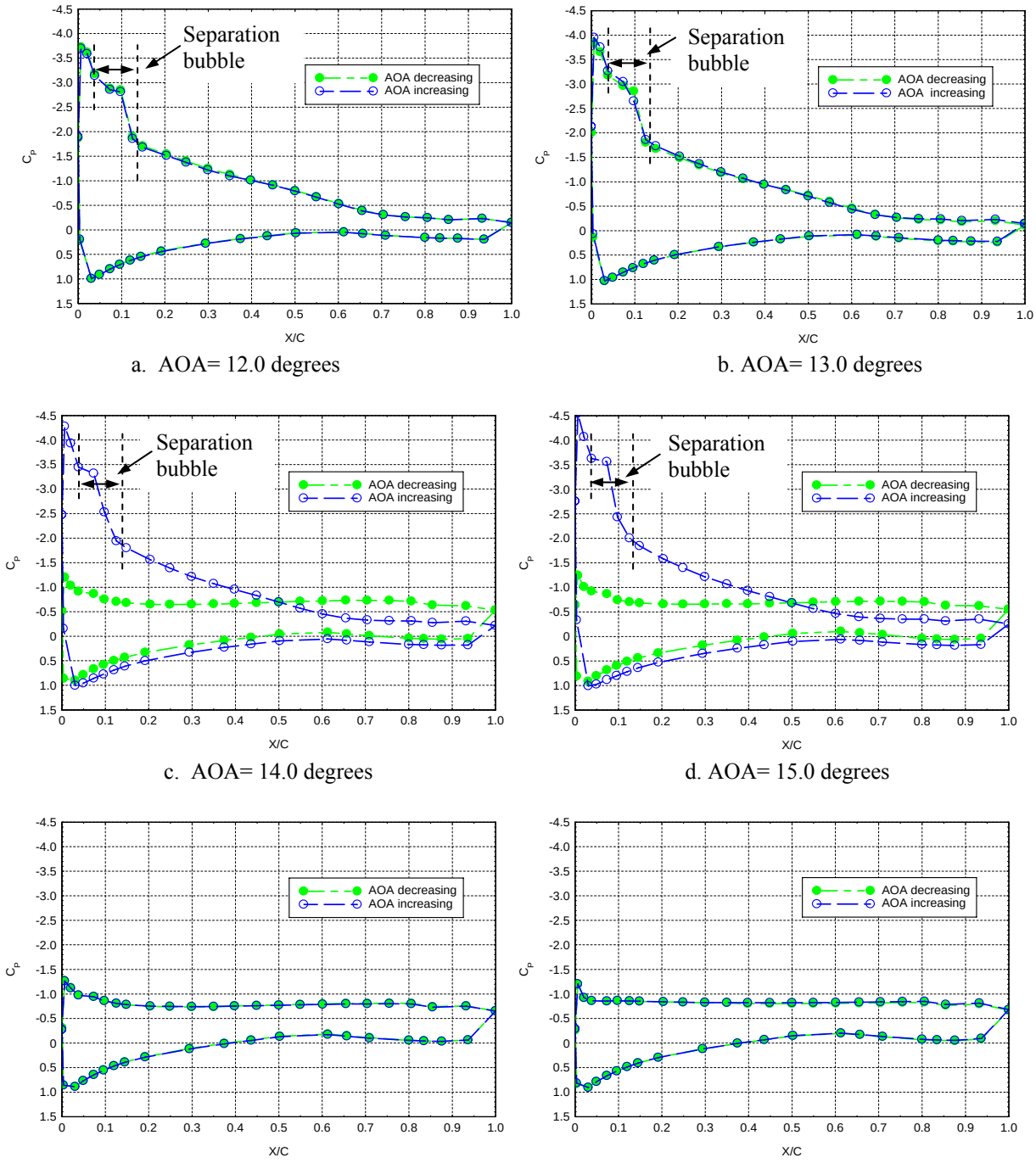

a. AOA= 12.0 degrees

b. AOA= 13.0 degrees

c. AOA= 14.0 degrees

d. AOA= 15.0 degrees

e. AOA= 16.0 degrees

f. AOA= 17.0 degrees

Fig. 4. Measured surface pressure distributions around the airfoil.

Based on the original ideas proposed by Horton [10], Russell [11] developed a theoretical model to characterize laminar separation bubbles formed on low-Reynolds-number airfoils, which is illustrated schematically in Fig. 5. Russell [10] suggested that the starting point of the pressure plateau indicates the location where the laminar boundary layer would separate from the airfoil upper surface (i.e., separation point). Since the transition of the separated laminar boundary layer to turbulence will result in a rapid pressure rise brought about by fluid entrainment, the termination of the pressure plateau could be used to locate the transition point (i.e., where the transition of the separated laminar boundary layer to turbulence would begin to occur). The pressure rise due to the

turbulence transition often overshoots the invisicid pressure that exists at the reattachment location. Therefore, the location of the point of equality between the actual and inviscid surface pressure marks the location of reattachment (i.e., reattachment point).

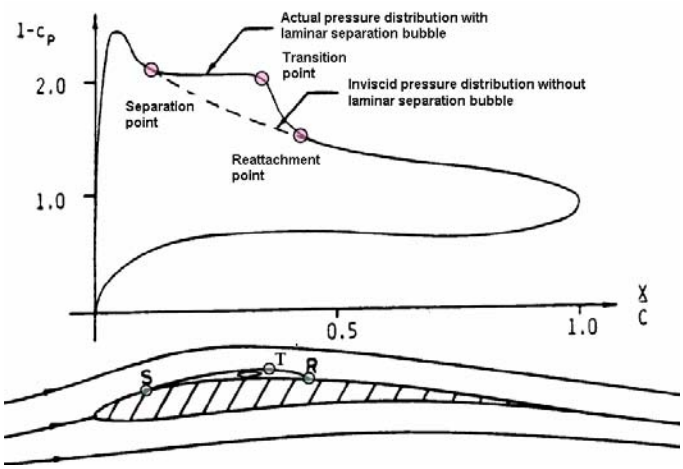

Fig. 5. Typical surface pressure distribution when a laminar separation bubble is formed (Russell [11])

Following the work of Russell [11], the locations of critical points (separation, transition, and reattachment points) at different angles of attack can be estimated based on the measured airfoil surface pressure profiles. Based in the measured surface pressure distribution given in Fig. 4, the separation, transition, and reattachment points at AOA=12.0 ~ 15.0 degrees were estimated to locate at *X/C* ≈ 0.05, X/C ≈ 0.8 and X/C ≈ 0.15 respectively. The length of the laminar separation bubble (i.e., the distance between the separation and reattachment points) was found to be about 10 % of the airfoil chord length, which is almost independent of the angle of attack.

When the airfoil angles of attach of AOA=14.0 and 15.0 degrees are at the decreasing angle branch of the hysteresis loop, the negative pressure coefficient peak near the airfoil leading edge was found to decrease significantly. The surface pressure over airfoil upper surface was found to be nearly constant. Such surface pressure distribution would indicate that large-scale flow separation has occurred over almost the entire upper surface of the airfoil, i.e., the airfoil is in stall state [12].

B. PIV measurement results

While the measurements of the surface pressure distributions and the lift and drag coefficients can be used to reveal the global characteristics of the aerodynamic hysteresis at the angles of attack close to the static stall angle of the low-Reynolds-number airfoil, quantitative flow field measurements taken by using the high-resolution PIV system can elucidate much more details about the significant differences in flow pattern and the behavior of vortex and turbulent flow structures around the airfoil when aerodynamic hysteresis occurs. In the present study, PIV measurements were conducted at two spatial resolution levels: a coarse level to visualize the global features of the flow pattern around the airfoil with the measurement window size being about 150mm×120mm; and a refined level to reveal further details about the transient behavior of the laminar boundary layer separation and transition near the nose of the airfoil with a measurement window size of about 40mm×30mm; The time interval between the double-pulsed laser illumination for the PIV measurements was set as Δt = 20.0μs, and 4.0μs. The effective resolutions of the PIV measurements (i.e., grid sizes) were Δ/C=0.018 and 0.0046.

Fig. 6 shows the PIV measurement results of the flow field around the low-Reynolds-number airfoil at AOA = 14.0 degrees in the term of instantaneous velocity field, ensemble-averaged velocity field, streamlines of the mean flow field and turbulent kinetic energy distribution when the 14.0 degrees angle of attack is at the increasing angle branch of the hysteresis loop. As visualized clearly from instantaneous and the mean velocity vector distributions, incoming flow streams were found to be able to attach to the airfoil upper surface in general when the 14.0 degrees angle of attack is at the increasing branch of the hysteresis loop. As described above, the measured surface pressure

distribution shown in Fig. 4 revealed that a separation bubble would be generated on the airfoil upper surface in the region of $X/C \approx 0.05\sim0.15$. Since the thickness of separation bubbles generated on low-Reynolds-number airfoils is usually very small, i.e., < 1% of the chord length (see Fig.8), the separation bubble could not be revealed clearly form the PIV measurement results given in Fig. 6 due to the limited spatial resolution of the PIV measurement (i.e., $\Delta/C = 0.018$). However, the existence of the separation bubble in the region of $X/C \approx 0.05\sim0.15$ can still be seen vaguely from the distributions of the mean velocity vectors and the corresponding streamlines. Since the incoming flow streams could attach to the airfoil upper surface in general, the wake region downstream of the airfoil is reasonably small. The small wake region would indicate a relatively small aerodynamic drag force acting on the airfoil, which is consistent with the measured airfoil drag coefficient data given in Fig.3.

Since the incoming flow streams could attach to the airfoil upper surface in general except in the small region near the airfoil leading edge where a separation bubble was formed, no apparent large-scale flow separation can be found in the flow field around the airfoil. As a result, the turbulent kinetic energy (*T.K.E.*) level of the flow field around the airfoil was found to be relatively low. The regions with relatively higher *T.K.E.* was found to concentrate in a thin layer close to the airfoil upper surface with the maximum value of the *T.K.E.* existing in the region where the separation bubble was generated.

Fig 7 shows the PIV measurement results when the 14.0 degrees angle of attack is at the decreasing angle branch of the hysteresis loop. The flow pattern around the airfoil was found to be completely different from that with 14.0 degrees angle of attack at the increasing angle branch of the hysteresis loop. As visualized clearly from the instantaneous PIV measurements results given in Fig. 7(a), laminar boundary layer (i.e., the thin vortex layer) affixing to the airfoil upper surface at the leading edge was found to separate from the airfoil upper surface at the location very near the airfoil leading edge. Strong unsteady vortex and turbulent structures were found to shed periodically in the wake of the airfoil after the separation of the laminar boundary layer. Both the mean velocity vectors and the corresponding streamlines reveal clearly that large-scale flow separation occurred on almost the entire upper surface of the airfoil, i.e., the airfoil is in stall state when the 14.0 degrees angle of attack was at the decreasing angle branch of the hysteresis loop. An interesting feature can be identified from the distribution of the streamlines is that the boundary layer separated from the airfoil upper surface near the airfoil leading edge seems to try to reattach to the airfoil upper surface at the location of $X/C \approx 0.35$. However, the strong reversing flow from the airfoil trailing edge prevented the separated boundary layer from reattaching to the airfoil upper surface and to keep the airfoil in stall state. Since the airfoil was found to be in stall state before it was changed to AOA=14.0 along the decreasing branch of the aerodynamic hysteresis loop, the flow field around the airfoil seems to be able to "remember" its past history (i.e., in stall state) when the angle of attack was changed inside the hysteresis loop. The large-scale flow separation on the airfoil upper surface caused the generation of a very large circulation region in the wake of the airfoil, which would indicate a significant aerodynamic drag force acting on the airfoil. This was confirmed again from the measured drag force data given in Fig. 3.

Since laminar boundary layer separated from the airfoil upper surface near the airfoil leading edge for good when the 14.0 degrees angle of attack was at the decreasing angle branch of the hysteresis loop, the separated boundary layer was found to transit to turbulence rapidly and generated strong unsteady vortex structures in the wake of the airfoil due to Kelvin-Helmholtz instabilities. The measured *T.K.E.* distribution given in Fig. 7 revealed clearly that the *T.K.E.* level of the flow field around the airfoil become significantly higher compared with the case with the 14.0 degrees angle of attack at the increasing angle branch of the hysteresis loop. The regions with higher *T.K.E.* were found to be along the shedding path of the strong unsteady Kelvin-Helmholtz vortex structures.

Although the PIV measurement results given in Fig. 6 and 7 revealed that the flow pattern and behavior of the vortex and turbulent flow structures around the airfoil with the angle of AOA=14.0 degrees at the decreasing angle branch of the hysteresis were significantly different from those with the same angle of attack of 14.0 degrees at increasing angle branch of the hysteresis loop, further details about the differences in the transient behavior of the behavior of the laminar boundary layer separation and transition near the leading edge of the low-Reynolds-number airfoil can not be seen clearly due to the limited spatial resolution of the PIV measurements. In order to provide further insights to elucidate underlying physics associated with aerodynamic hysteresis of low-Reynolds-number airfoils, refined PIV measurements near the nose of the airfoil with much higher spatial resolution ($\Delta/C = 0.0046$) were carried out. The measurement results are shown in Fig. 8 and Fig. 9 with the angle of attack of 14.0 degrees at the decreasing angle branch and increasing angle branch of the hysteresis loop respectively.

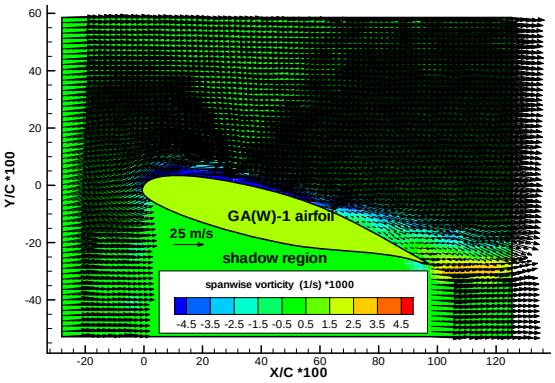

a. Instantaneous velocity field

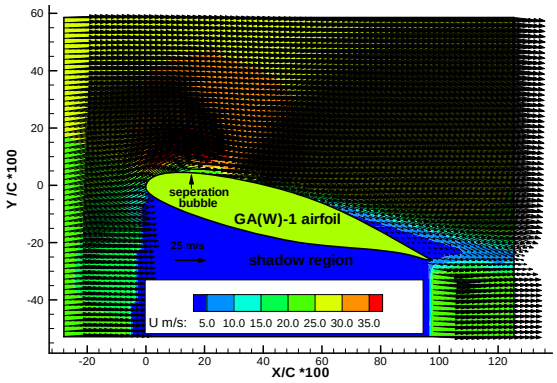

b. Ensemble-averaged velocity field

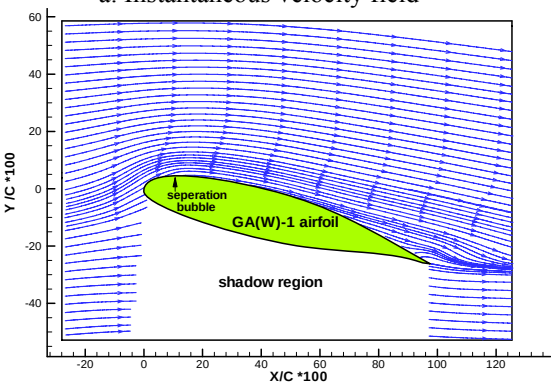

c. Streamlines of mean flow field

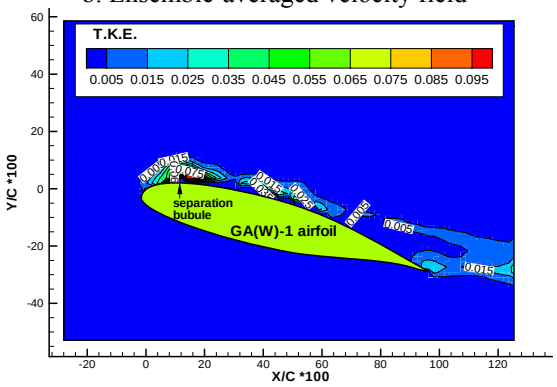

d. Turbulent kinetic energy distribution

Fig 6. PIV measurement results with AOA=14.0 degrees at the increasing branch of the hysteresis loop

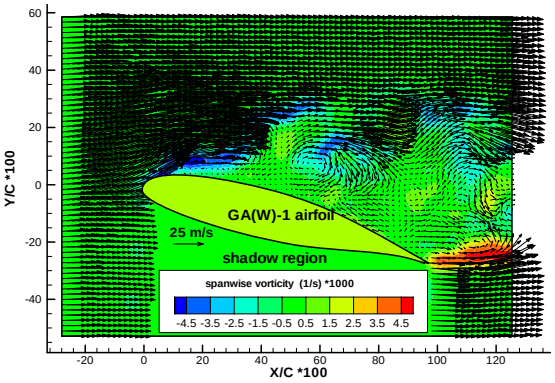

a. Instantaneous velocity field

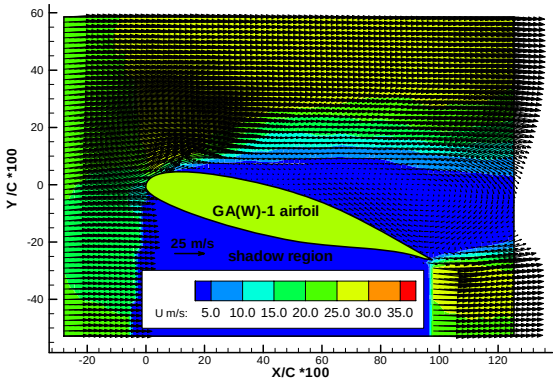

b. Ensemble-averaged velocity field

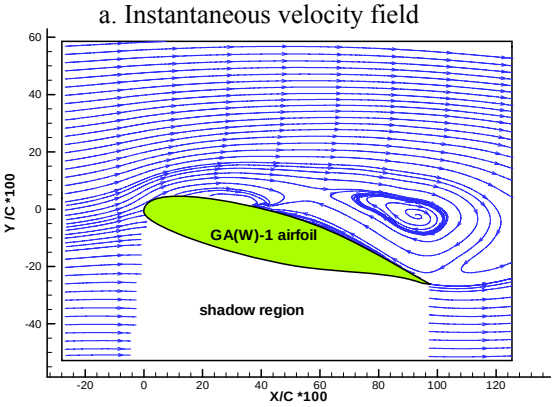

c. Streamlines of mean flow field

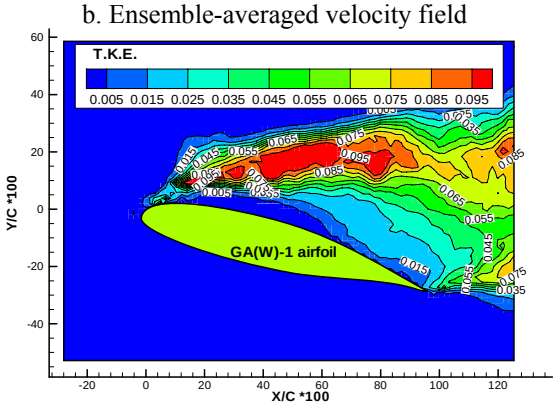

d. Turbulent kinetic energy distribution

Fig 7. PIV measurement results with AOA=14.0 degrees at the decreasing branch of the hysteresis loop

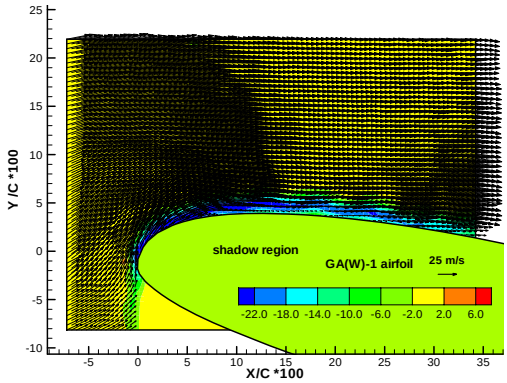

a. Instantaneous velocity field

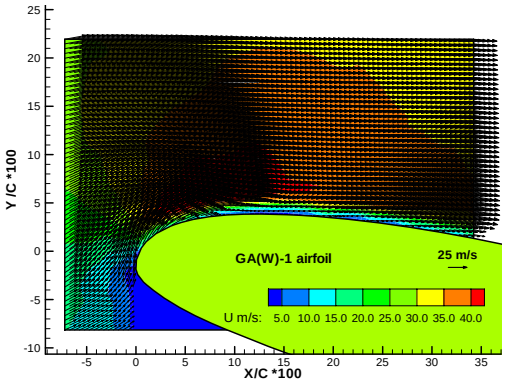

b. Ensemble-averaged velocity field

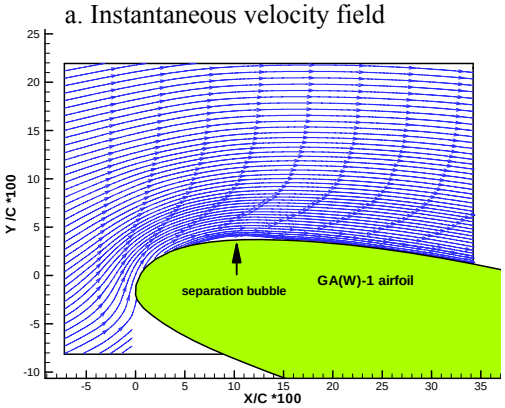

c. Streamlines of mean flow field

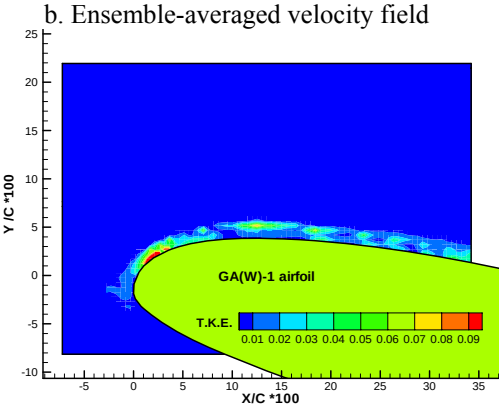

d. Turbulent kinetic energy distribution

Fig 8. Refined PIV measurement results with AOA=14.0 degrees at the increasing branch of the hysteresis loop

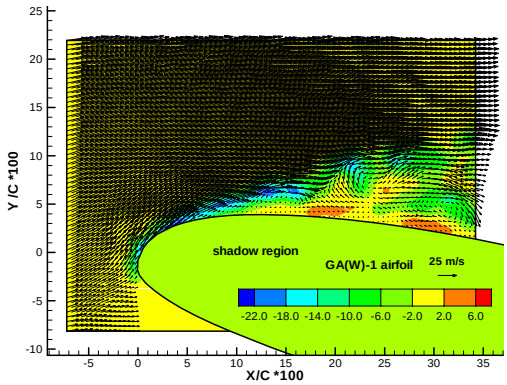

a. Instantaneous velocity field

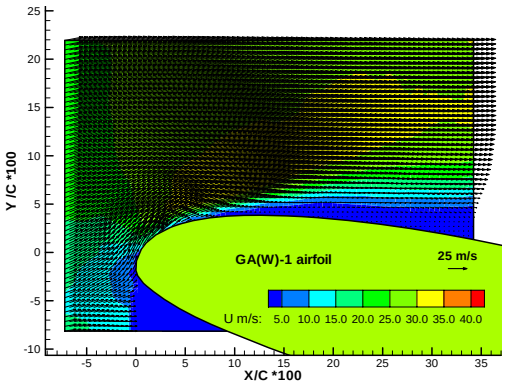

b. Ensemble-averaged velocity field

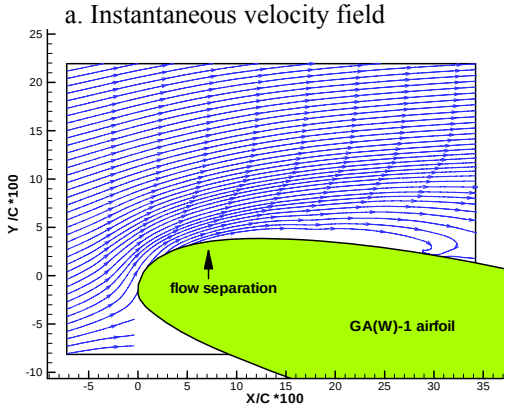

c. Streamlines of mean flow field

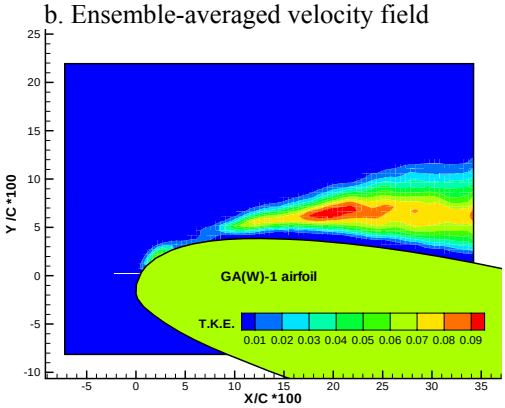

d. Turbulent kinetic energy distribution

Fig 9. Refined PIV measurement results with AOA=14.0 degrees at the increasing branch of the hysteresis loop.

When the 14.0 degrees angle of attack is at the increasing angle branch of the hysteresis loop, a laminar boundary layer was revealed clearly in Fig. 8 as a thin vortex layer affixing to the airfoil surface in the instantaneous PIV measurement results. The laminar boundary layer was found to attach to the airfoil upper surface near the airfoil leading edge, as it is expected. Because of the severe adverse pressure gradient on the airfoil upper surface at AOA =14.0 degrees as revealed from the surface pressure measurement data given in Fig. 3, the laminar boundary layer (i.e., the thin vortex layer) was found to separate slightly from the airfoil upper surface at first, then reattach to the airfoil surface at a downstream location, which results in the formation of a separation bubble between the separation point and the reattachment point. Time sequence of instantaneous PIV measurements reveals clearly that, while the locations of the separation points and reattachment points varied dynamically from one frame to another, most of the separation points were found to be located at X/C ≈ 0.05 and reattachment points at X/C ≈ 0.15. The formation of the separation bubble can be seen more clearly from the ensemble-averaged velocity field and the streamlines of the mean flow field. Based on the PIV measurement results, the location of the separation point (i.e., from where the streamlines of the mean flow would separate from the airfoil upper surface) was found to be in the neighborhood of $X/C \approx 0.05$, which agrees well with the starting point of the pressure plateau in the measured airfoil surface pressure profile as the 14.0 degrees angle of attack is at the increasing angle branch of the hysteresis loop. The PIV measurements revealed that the reattachment point (i.e., where the separated streamline would reattach to the airfoil upper surface) was in the neighborhood of $X/C \approx 0.15$, which also agrees well with the estimated location of the reattachment point based on the airfoil surface pressure measurements. While the total length of the separation bubble was found to be about 10% of the airfoil chord length, the separation bubble was found to be very thin, only about ~1% of the chord length in height.

As revealed clearly in the PIV measurement results given in Fig. 9, laminar boundary layer on the airfoil upper surface was found to separate from the upper surface of the airfoil for good from the location very near to the airfoil leading edge when the 14.0 degrees angle of attack is at the decreasing angle branch of the hysteresis loop. The separated laminar boundary layer was found to transit to turbulence rapidly by rolling up strong unsteady vortex structures due to the Kelvin-Helmholtz instabilities. The separated boundary layer was found to be "lifted" up far away from the upper surface of the airfoil. As described above, the streamline distribution of the mean flow field elucidate that the separated boundary layer seems to try to reattach to the airfoil upper surface at the location of $X/C \approx 0.30$. However, the strong reversing flow from the airfoil trailing edge prevented the separated boundary layer from reattaching to the airfoil upper surface and to keep the airfoil in stall state, which is visualized clearly from the PIV measurement results.

IV. Concluding Remarks

An experimental study was conducted to investigate the aerodynamic hysteresis near the static stall angle of a NASA low-speed GA(W)-1 airfoil. The experimental investigation was conducted in a closed-circuit low-speed wind tunnel with the chord Reynolds number of $Re_C = 160{,}000$. In addition to mapping surface pressure distribution around the airfoil with pressure sensors, a high-resolution particle image velocimetry (PIV) system was used to make detailed flow field measurements to quantify the occurrence and behavior of laminar boundary layer separation and transition on the airfoil when aerodynamic hysteresis occurs. The flow field measurements were correlated with the airfoil surface pressure measurements to elucidate underlying fundamental physics associated with the aerodynamic hysteresis phenomena of low-Reynolds number airfoils.

The measurement result revealed clearly that, for the same angle of attack in the hysteresis loop, incoming flow streams were to be able to attach to the airfoil upper surface in general when the angle is at the increasing branch of the hysteresis loop. The attached flow pattern resulted in higher lift and lower drag acting on the airfoil as well as small unsteadiness in the wake of the airfoil. When the angles of attack is at the decreasing branch of the hysteresis loop, incoming flow streams were found to separate from the airfoil upper surface for good at a location very near to the leading edge of the airfoil. Strong vortex structures were found to shed periodically in the wake of the airfoil. Large-scale flow separation was found to take place almost on the entire upper surface of the airfoil. As a result, the lower lift and higher drag acting on the airfoil were found with the unsteadiness in the wake of the airfoil increased significantly. The present study revealed quantitatively that aerodynamic hysteresis of low-Reynolds number airfoils is closely related to the behavior of the laminar boundary layer separation and transition on the airfoils. The ability of the flow to remember its past history is responsible for the hysteretic behavior.

Acknowledgments

The authors also want to thank Mr. Bill Rickard of Iowa State University for their help in conducting the experiments. The support of National Science Foundation CAREER program under award number of CTS-0545918 is gratefully acknowledged.

References

[1]. Carmichael, B. H., "Low Reynolds number airfoil survey", Vol. 1, NASA CR-165803, 1981.

[2]. McCorskey, W.J., "Unsteady airfoil", Ann. Rev. Fluid Mech. Vol. 14, 1982, pp285-311.

[3]. Pohlen, L. J., and Mueller, T. J.," Boundary Layer Characteristics of the Miley Airfoil at Low Reynolds Numbers", Journal of Aircraft, Vol. 21, No.9, 1984, pp658-664.

[4]. Mueller, T. J., "The influence of laminar separation and transition on low Reynolds number airfoil hysteresis" , Journal of Aircraft, Vol. 22, No. 9, 1985, pp763-770.

[5]. Hoffmann, J. A., "Effects of freestream turbulence on the performance characteristics of an airfoil," AIAA Journal, Vol. 29, No.9, 1991, pp. 1353-1354.

[6]. Biber, K., and G. W. Zumwalt, "Hysteresis Effect on Wind Tunnel Measurements of a Two-Element Airfoil", Vol. 31, No.2, 1993, pp326-330

[7]. Mittal, S. and Saxena P., "Prediction of hysteresis associated with static stall of an airfoil", AIAA Journal, Vol. 38, No. 5, 2002, pp933-935.

[8]. Thibert, J. J., Grandjacques, M., and Ohman, L. H., "Experimental database for computer program assessment," TR AR-138, AGARD, May1979.

[9]. Rogers, E. W. E., "Blockage Effects in Closed or Open Tunnels," AGARDO graph 109, 1966, pp. 279-340.

[10]. Horton, H.P., "A Semi-Empirical Theory for the Growth and Bursting of Laminar Separation Bubbles," British ARC CP 1073, June, 1969.

[11]. Russell, J., "Length and Bursting of Separation Bubbles: A Physical Interpretation", Science and Technology of Low Speed Motorless Flight, NASA Conference Publication 2085, Part 1, 1979.

[12]. O'Meara, M. M., and Mueller, T. J. "Laminar separation bubble characteristic on an airfoil at low Reynolds numbers", AIAA Journal, Vol. 25, No. 8, 1987, pp1033-1041.